PHYSICAL REVIEW B
CONDENSED MATTER

THIRD SERIES, VOLUME 36, NUMBER 8 15 SEPTEMBER 1987-I

Electron-phonon interaction effects in tantalum

Abdrabuh Al-Lehaibi* and James C. Swihart
Department of Physics, Indiana University, Bloomington, Indiana 47405

William H. Butler
Metals and Ceramics Division, Oak Ridge National Laboratory, Oak Ridge, Tennessee 37831

Frank J. Pinski
Department of Physics, University of Cincinnati, Cincinnati, Ohio 45221
(Received 4 February 1987)

The results of calculations for a number of electron-phonon interaction effects for tantalum are presented. The calculations are based on Korringa-Kohn-Rostoker energy bands, Born–von Kármán phonons, and the rigid-muffin-tin approximation for the electron-phonon matrix element. The calculated Eliashberg spectral function α^2F is compared with the earlier tunneling data of Shen and the proximity tunneling data of Wolf *et al.* The calculated and tunneling transverse-phonon peaks agree well, but the height of the tunneling longitudinal-phonon peak is smaller than the calculated results. The calculated electron-phonon coupling parameter λ is 0.88, which is larger than the λ determined from superconducting tunneling and superconducting T_c measurements, but is slightly smaller than the λ determined from electronic specific-heat measurements. Calculated phonon linewidths along various symmetry directions are presented. The temperature dependence of the electrical resistivity due to phonon scattering is calculated in the lowest-order variational approximation and it agrees with experiment. The point-contact spectral function of Kulik, $G(\omega)$, is determined and compared with $\alpha^2F(\omega)$. The agreement between calculated and measured electronic specific heat and high-temperature electrical resistivity gives strong support to the validity of the rigid-muffin-tin approximation for electron-phonon matrix elements. The main disagreement between calculated and measured results is for superconducting properties for which an *ad hoc* Coulomb interaction μ^* must be used.

I. INTRODUCTION

In recent years it has become possible to perform detailed calculations of electron-phonon effects in both simple metals and transition metals. Such calculations typically use realistic electronic structures, a realistic description of the phonons, and realistic models of the electron-phonon matrix elements. Examples of quantities calculated using realistic models are phonon linewidths in Nb,[1] the anisotropic electronic lifetime in Al,[2] Cu,[3] and In,[4] the anisotropic mass enhancement in Zn,[5] Cu,[3] and In,[6] the electrical resistivity of Al,[7] Zn,[8] Nb,[9] Pd,[9] Cu,[10] and the hexagonal metals Zn, Cd, and Mg,[11] the thermal resistivity in Al,[7] Zn,[8] Nb,[9], Pd,[9] and Cu,[10] the point-contact spectral function $G(\omega)$ of Kulik[12] for the alkali metals,[13,14] and the superconducting transition temperature[15] T_c for V, Nb, Ta, Mo, W, Pd, and Pb.

Many of these calculations first involve determining the Eliashberg spectral function $\alpha^2F(\omega)$. Although $\alpha^2F(\omega)$ is not a directly observable quantity, it enters into the gap equation that determines the superconducting transition temperature. In strong-coupling superconductors it has been possible to deduce α^2F from tunneling data.[16] To our knowledge, there are only three cases for the simple metals for which $\alpha^2F(\omega)$ has been both calculated for realistic models [calculations on Pb (Refs. 15 and 17), In (Ref. 18), Al (Ref. 19)] and also determined experimentally. The calculated $\alpha^2F(\omega)$ agrees well in each case with that determined from tunneling[16] or from proximity-effect tunneling measurements.[20] On the other hand, Nb is the only transition metal for which there exist calculations[1,15,21,22] together with experimental determinations from proximity-effect tunneling[23] and ordinary tunneling[24] of α^2F. (In the work of Ref. 15, α^2F is presumably calculated for Ta; however, the results are not presented in the published paper.) For Nb there is a marked disagreement between the calculations and the results deduced from the tunneling experiments. The lower-energy transverse peak

 ©1987 The American Physical Society

in α^2F for Nb is essentially the same in location, height, shape, and width whether determined by direct calculation or from tunneling experiments, and the longitudinal peak occurs at the same energy independent of the method. However, the strength of the longitudinal peak determined from tunneling experiments is smaller than that determined from direct calculations. Possible reasons for this suppression have been suggested.[23,25,26]

The most central and problematic aspect of these calculations is the determination of the electron-phonon matrix elements. Although this problem seems to be well understood in principle[27] (i.e., it is known that the electron-phonon matrix elements should be calculated from the change in the charge self-consistent crystal potential caused by an infinitesimal displacement of a single nucleus in an otherwise perfect crystal[28–30]), in practice approximations are usually required for actual calculations. In addition it is often difficult to assess the degree of success of a particular approximation for the electron-phonon matrix elements. Usually there are other approximations involved in the calculation, and the interpretation of most experimental determinations of the strength of the electron-phonon interaction is not completely straightforward.

In this paper the "rigid-muffin-tin" approximation (RMTA) is used to calculate the electron-phonon matrix elements of Ta. This approximation applies the rigid shift of one of the muffin-tin potentials used to calculate the electronic structure of the perfect crystal instead of the change in the self-consistent crystal potential effected by the displacement of a single atom. Although this approximation may be criticized as *ad hoc* it has the feature of being a "first-principles" method in the sense that the matrix elements are calculated from the electronic structure and no adjustable parameters are involved. It also has the virtue that it satisfies the total-force sum rule.[31]

In order that we may assess the validity of the RMTA we have attempted to perform the remainder of the calculation as carefully as possible. We have used a self-consistent, relativistic potential to calculate the electronic structure, and have generated wave vectors and wave functions on a dense mesh of points at the Fermi energy. The frequencies and polarizations that enter the calculations were obtained from Born–von Kármán fits to the experimental phonon dispersion curves.

We are also interested in testing a second transition-metal superconductor to see whether or not the same suppression of the longitudinal peak in α^2F occurs according to tunneling data, as is the case for Nb. Tantalum is a good candidate because there exist good experimental tunneling data[26,32] and proximity-effect tunneling data[33] from which $\alpha^2F(\omega)$ has been determined. We present here our calculations of $\alpha^2F(\omega)$ for Ta for comparison with the tunneling α^2F.

We have also calculated a wide range of other properties that may be compared with experiment. A very important measure of the electron-phonon interaction is the temperature-dependent electrical resistivity. The linear coefficient of the electrical resistivity at temperatures greater than the Debye temperature is a good measure of the overall strength of the electron-phonon coupling, and the temperature dependence contains information about the frequency dependence of the coupling. One of the most direct measures of the electron-phonon interaction is the phonon linewidth. This function gives the contribution of each phonon mode to the coupling. We also calculate the point-contact spectral function which contains information similar to that contained in the Eliashberg spectral function.

In Sec. II we discuss our model and method of calculation. In Sec. III we present the results; then in Sec. IV we present our conclusions.

II. METHOD OF CALCULATION

The calculations discussed in this paper are based on techniques described previously[1,9,34] so only a brief discussion will be presented here. The process of calculating the electron-phonon parameters involves several separate steps. First the electronic structure in the vicinity of the Fermi energy must be determined. Then matrix elements must be calculated for scattering between various points on the Fermi surface. Finally, the electronic information and the phonon frequencies and polarization vectors must be combined and properly averaged to generate the quantities of interest.

The electronic structure problem is solved by using a Korringa-Kohn-Rostoker (KKR) band-theory program operated in a constant-energy mode.[34] The muffin-tin potential that we used for our calculations on Ta was one determined self-consistently in Ref. 35 using $X\alpha$ exchange. Operating in a constant-energy mode allows us to efficiently generate many points on the Fermi surface of Ta without having to resort to linearized schemes or interpolation methods. The wave-function coefficients are determined simultaneously with the k vectors. The primary difference between the present electronic structure calculations and those reported in Refs. 1, 9, and 34 is that in this paper we include relativistic effects[36,37] (omitting the spin-orbit interaction).

After the Fermi-energy electronic structure is obtained, the wave-function coefficients are used to calculate the electronic part of the electron-phonon matrix elements in the rigid-muffin-tin approximation:[1]

$$I^{\alpha}_{\mathbf{k}\mathbf{k}'}=\langle \psi_{\mathbf{k}} \mid \hat{\mathbf{x}}_{\alpha}\cdot\nabla V \mid \psi_{\mathbf{k}'}\rangle \ , \tag{1}$$

where $\psi_{\mathbf{k}}$ is a Fermi-energy Bloch function, $\hat{\mathbf{x}}_{\alpha}$ is a direction cosine, and V is the muffin-tin potential used in the band calculations. The square of $I^{\alpha}_{\mathbf{k}\mathbf{k}'}$ is then averaged over both $\mathbf{k}$ and $\mathbf{k}'$ on the Fermi surface taking care to distinguish all scattering processes with different values of $\mathbf{q}$ where $\mathbf{q}=\mathbf{k}-\mathbf{k}'$:

$$\eta_{\alpha\beta}(\mathbf{q})=\frac{(2\pi)^3}{\Omega_a N(\varepsilon_F)}\sum_{\mathbf{k},\mathbf{k}'}\delta(\varepsilon_F-\varepsilon_{\mathbf{k}})\delta(\varepsilon_F-\varepsilon_{\mathbf{k}'}) \times\delta(\mathbf{k}-\mathbf{k}'-\mathbf{q})I^{\alpha}_{\mathbf{k}\mathbf{k}'}I^{\beta}_{\mathbf{k}'\mathbf{k}} \ . \tag{2}$$

Here $N(\varepsilon_F)$ is the Fermi-energy density of states and Ω_a is the volume per atom. In carrying out the double sum in Eq. (2) of $\mathbf{k}$ and $\mathbf{k}'$ over the Fermi surface, we use a

mesh of points on the irreducible ($\frac{1}{48}$th) Fermi surface. $\mathbf{k}$ is confined to the $\frac{1}{48}$th part but $\mathbf{k}'$ is determined on all points on the Fermi surface by first locating a mesh point on the irreducible part and then carrying out the point operations of O_H symmetry to generate 48 $\mathbf{k}'$ points for each mesh point.

Once Eq. (2) has been evaluated, the quantity $\eta_{\alpha\beta}(\mathbf{q})$ can be used to derive the electron-phonon parameters. The phonon linewidth arising from the electron-phonon interaction is given, for example, by

$$\gamma_j(\mathbf{q})=\frac{\pi\hbar}{M_a}N(\varepsilon_F)\sum_{\alpha,\beta}\epsilon_\alpha^j(\mathbf{q})\epsilon_\beta^j(\mathbf{q})\eta_{\alpha\beta}(\mathbf{q}) , \tag{3}$$

where M_a is the atomic mass and $\epsilon_\alpha^j(\mathbf{q})$ is the αth component ($\alpha=1,3$) of the phonon-polarization vector of polarization j. The phonon frequencies and polarization vectors are obtained from a Born–von Kármán fit to the experimental dispersion curves of Ref. 38. Similarly, the Eliashberg electron-phonon spectral function $\alpha^2F(\omega)$ is given by

$$\alpha^2F(\omega)=\frac{1}{M_a}\sum_{\alpha,\beta}\sum_{\mathbf{q}}\sum_{j}\epsilon_\alpha^j(\mathbf{q})\epsilon_\beta^j(\mathbf{q})\eta_{\alpha\beta}(\mathbf{q})\delta(\omega^2-\omega_{\mathbf{q}j}^2) , \tag{4}$$

where $\omega_{\mathbf{q}j}$ is the frequency of a phonon with wave vector $\mathbf{q}$ and mode index or polarization j.

The electron-phonon parameters associated with transport can be obtained from quantities defined similarly to $\eta_{\alpha\beta}(\mathbf{q})$, but which include the Fermi velocities:

$$\eta_{\alpha\beta}^{\text{out}}(\mathbf{q})=\frac{(2\pi)^3}{\Omega_a}\frac{\sum_{\mathbf{k},\mathbf{k}'}\delta(\varepsilon_F-\varepsilon_{\mathbf{k}})\delta(\varepsilon_F-\varepsilon_{\mathbf{k}'})\delta(\mathbf{k}-\mathbf{k}'-\mathbf{q})I_{\mathbf{k}\mathbf{k}'}^{\alpha}I_{\mathbf{k}'\mathbf{k}}^{\beta}v_{\mathbf{k}}^2}{\sum_{\mathbf{k}}\delta(\varepsilon_F-\varepsilon_{\mathbf{k}})v_{\mathbf{k}}^2} , \tag{5}$$

$$\eta_{\alpha\beta}^{\text{in}}(\mathbf{q})=\frac{(2\pi)^3}{\Omega_a}\frac{\sum_{\mathbf{k},\mathbf{k}'}\delta(\varepsilon_F-\varepsilon_{\mathbf{k}})\delta(\varepsilon_F-\varepsilon_{\mathbf{k}'})\delta(\mathbf{k}-\mathbf{k}'-\mathbf{q})I_{\mathbf{k}\mathbf{k}'}^{\alpha}I_{\mathbf{k}'\mathbf{k}}^{\beta}\mathbf{v}_{\mathbf{k}}\cdot\mathbf{v}_{\mathbf{k}'}}{\sum_{\mathbf{k}}\delta(\varepsilon_F-\varepsilon_{\mathbf{k}})v_{\mathbf{k}}^2} . \tag{6}$$

Here $\mathbf{v}_{\mathbf{k}}$ is the group velocity of an electron at point $\mathbf{k}$ on the Fermi surface. The results of Eqs. (5) and (6) may be used to calculate the transport spectral function $\alpha_{\text{tr}}^2F(\omega)$ and the electrical resistivity in the lowest-order variational approximation (LOVA). Explicitly,

$$\alpha_{\text{tr}}^2F(\omega)=\frac{1}{M_a}\sum_{\alpha,\beta}\sum_{\mathbf{q}}\sum_{j}\epsilon_\alpha^j(\mathbf{q})\epsilon_\beta^j(\mathbf{q})\delta(\omega^2-\omega_{\mathbf{q}j}^2)\times[\eta_{\alpha\beta}^{\text{out}}(\mathbf{q})-\eta_{\alpha\beta}^{\text{in}}(\mathbf{q})] \tag{7}$$

and

$$\rho_{\text{LOVA}}=\frac{6\pi k_BT}{e^2\hbar N(\varepsilon_F)\langle v^2\rangle}\int_0^\infty\frac{d\omega}{\omega}\frac{x^2}{\sinh^2x}\alpha_{\text{tr}}^2F(\omega) . \tag{8}$$

Here x is $\hbar\omega/2k_BT$, and $\langle v^2\rangle$, the mean square Fermi velocity, is given by

$$\langle v^2\rangle=[N(\varepsilon_F)]^{-1}\sum_{\mathbf{k}}\delta(\varepsilon_F-\varepsilon_{\mathbf{k}})v_{\mathbf{k}}^2 . \tag{9}$$

The point-contact spectral function of Kulik[12] $G(\omega)$ is closely related to the transport spectral function. It is defined by

$$G(\omega)=\frac{1}{M_a}\sum_{\alpha,\beta}\sum_{\mathbf{q}}\sum_{j}\epsilon_\alpha^j(\mathbf{q})\epsilon_\beta^j(\mathbf{q})\eta_{\alpha\beta}^{\text{PC}}(\mathbf{q})\delta(\omega^2-\omega_{\mathbf{q}j}^2) , \tag{10}$$

where the point-contact η^{PC} given by

$$\eta_{\alpha\beta}^{\text{PC}}(q)=\frac{(2\pi)^3}{\Omega_aN(\varepsilon_F)}\sum_{\mathbf{k},\mathbf{k}'}\delta(\varepsilon_F-\varepsilon_{\mathbf{k}})\delta(\varepsilon_F-\varepsilon_{\mathbf{k}'})\times\delta(\mathbf{k}-\mathbf{k}'-\mathbf{q})K(\mathbf{v},\mathbf{v}')I_{\mathbf{k}\mathbf{k}'}^{\alpha}I_{\mathbf{k}'\mathbf{k}}^{\beta} \tag{11}$$

is similar to $\eta_{\alpha\beta}$ of Eq. (2) but with the addition of the "geometrical structure factor"

$$K(\mathbf{v},\mathbf{v}')=\frac{|v_z||v_z'|}{|\mathbf{v}v_z'-\mathbf{v}'v_z|}\Theta(-v_zv_z') , \tag{12}$$

where $\mathbf{v}$ ($\mathbf{v}'$) is the electron velocity for state $\mathbf{k}$ ($\mathbf{k}'$), and v_z is the component of the velocity normal to the plane of the point contact. The function $\Theta(x)$ is the usual step function, which ensures that the only scatterings which contribute are those in which the electron reverses direction with respect to the point contact.

The geometrical structure factor [Eq. (12)], which weights large-angle scatterings more heavily than small-angle scatterings, obviously diverges for 180° scattering ($\mathbf{k}'=-\mathbf{k}$), but the sum over $\mathbf{k}$ and $\mathbf{k}'$ in Eq. (11) is nevertheless convergent. However, because of this divergence, care must be taken in carrying out the $\mathbf{k},\mathbf{k}'$ sum in (11). We have evaluated this sum in two different ways for a given number of mesh points on the Fermi surface. First, we evaluated Eq. (11), throwing out (i.e., setting equal to zero) all contributions in which $\mathbf{k}'$ is exactly equal to $-\mathbf{k}$. Next we reevaluated Eq. (11), and each time we encountered a case of $\mathbf{k}'$ exactly equal to $-\mathbf{k}$, we changed the direction of $\mathbf{k}'$ slightly in a random way using a random number generator. We compared the results for the two methods of evaluation and with the mesh-size parameter N_s equal to 12 and 24 (the latter corresponding to 5.07×10^6 $\mathbf{k},\mathbf{k}'$ pairs), and in this way determined that the results were converged.

III. RESULTS

Table I shows the calculated Fermi-energy density of states decomposed according to irreducible representation.

TABLE I. Calculated Fermi-energy density of states for Ta. Comparison is made with previous work of Ref. 35. See text for an explanation of the differences.

Angular momentum component	Present work (states/spin Ry)	Ref. 35 (states/spin Ry)
s	0.152	0.129
p	1.702	1.834
$d_{25'}$	4.729	4.959
d_{12}	1.027	1.058
f_{25}	0.282	
f_{15}	0.110	
f_2	0.026	
f_p	0.015	
Total	8.043	7.980

Our results are compared with the results of Boyer *et al.*,[35] who used a Slater-Koster tight-binding parametrization scheme for analyzing the Fermi surface. The total densities of states are in excellent agreement. The differences in the component densities of states are primarily due to the fact that the two techniques decompose the density of states in fundamentally different ways. In the KKR method the entire density of states within a cell is expanded in terms of angular momentum basis functions centered at the cell center. In the tight-binding method, on the other hand, the tails of functions on one site that extend into neighboring sites maintain their original identity as s, p, or d states even though they would contribute to different types of symmetry if they were expanded about the center of the cell they are in.

The total Fermi-energy density of states of 8.04 states/Ry spin may be compared with the enhanced density of states deduced from the linear term in the low-temperature electronic specific heat using the relation

$$C_v^e = \tfrac{2}{3}\pi^2 k_B^2 T N^*(E_F) \ . \tag{13}$$

The values of the enhanced Fermi-energy density of states $N^*(E_F)$ determined from Eq. (13) using experimental values for C_v^e vary from 15.7 states/Ry spin (Ref. 39) to 17.2 states/Ry spin.[40] These experimental values of the density of states are enhanced by the factor $1+\lambda$ over the band density of states where λ is the electron-phonon mass enhancement parameter. Thus dividing these values by our calculated density of states yields the enhancement factor $1+\lambda = N^*(E_F)/N(E_F)$. The value of λ necessary to make the experimental enhanced density of states consistent with the calculated band density of states is between 0.95 and 1.14. This is in reasonably good agreement with our calculated value for λ of 0.88.

In Fig. 1 our calculated Eliashberg spectral function $\alpha^2F(\omega)$ for Ta is plotted, together with the results from tunneling[26,32] and from proximity-effect tunneling experiments.[33] As in the case of Nb, there is fairly good agreement between the calculated transverse-phonon peak and that determined from the two experimental methods. The experimental curves are slightly larger than the calculation at low frequencies (in the neighborhood of 7 meV).

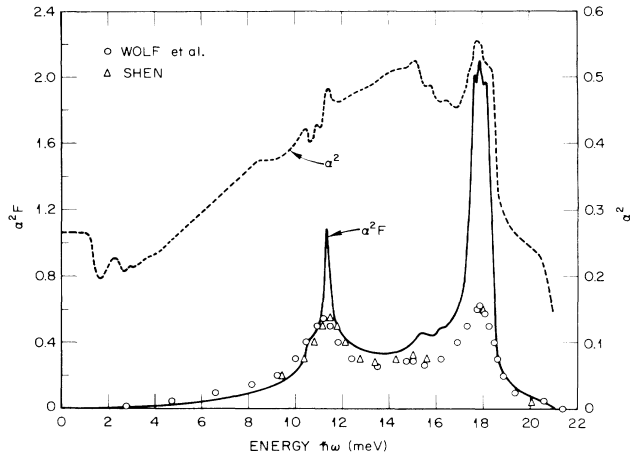

FIG. 1. Eliashberg spectral function $\alpha^2F(\omega)$ and frequency-dependent electron-phonon coupling parameter $\alpha^2(\omega)$ for Ta. The solid line is our calculated function $\alpha^2F(\omega)$ while the dashed line is $\alpha^2(\omega)$. The open circles are from Ref. 33 using proximity-effect tunneling results, while the open triangles are from Refs. 26 and 32 using tunneling. The two experimental curves are so close to each other that we have not drawn in the triangles over much of the energy range.

However, the calculated transverse peak is larger and sharper than the analyzed experiments. In the region between the two peaks the calculated result is slightly larger than experiment.

We remark that the overall agreement is very good and the disagreements are relatively minor for $\omega < 15$ meV. As with Nb, the main disagreement is at the longitudinal peak where the calculated result is much larger than that from tunneling. Unlike the case with Nb, the longitudinal peak from tunneling is slightly larger than the transverse peak. It is only in comparing the tunneling longitudinal peak with the calculated longitudinal peak that it becomes apparent that the tunneling peak is suppressed.

From $\alpha^2F(\omega)$, we determine λ, which is a good measure of the overall strength of the electron-phonon interaction; it is given by

$$\lambda = 2\int \frac{\alpha^2F(\omega)}{\omega} d\omega \ . \tag{14}$$

Our calculated result for Ta is $\lambda = 0.877$ compared to $\lambda = 0.69$ from the analysis both of tunneling[32] and proximity-effect tunneling experiments.[33]

Table II lists some of the calculated electronic parameters related to the superconducting transition. See Ref. 41 for the definitions of $\langle\omega^2\rangle^{1/2}$ and $\omega_{\log}$. The superconducting transition temperature T_c is calculated using $\omega_{\log}$ and $\mu^* = 0.13$ in the Allen-Dynes formula.[41] In this table we compare with calculated values for Ta from Ref. 42. The calculated value of $T_c = 7.01$ K is to be compared with the experimental value of 4.5 K.[43]

We have calculated the phonon linewidths for various phonons in Ta by means of Eq. (3). These are plotted in Fig. 2. We have carried out these calculations for the longitudinal and both transverse modes along the three symmetry directions [100], [110], and [111]. The results are

TABLE II. Calculated values of electronic parameters related to the superconducting transition and transport in tantalum. For the superconducting transition temperature T_c, the Coulomb pseudopotential μ^* is set at 0.13 and $\omega_{\log}$ is used in the Allen-Dynes formula of Ref. 41.

	$\langle\omega^2\rangle^{1/2}$ (K)	$\omega_{\log}$ (K)	λ	η (eV/Å^2)	T_c (K)	λ_{tr}	$N(E_F)$ (states/spin Ry)	E_F (Ry)
Present work	166.5	150.8	0.88	7.82	7.01	0.572	8.04	0.6972
Ref. 42	148		1.05	7.40			8.29	0.6924
Expt: Ref. 43					4.5			

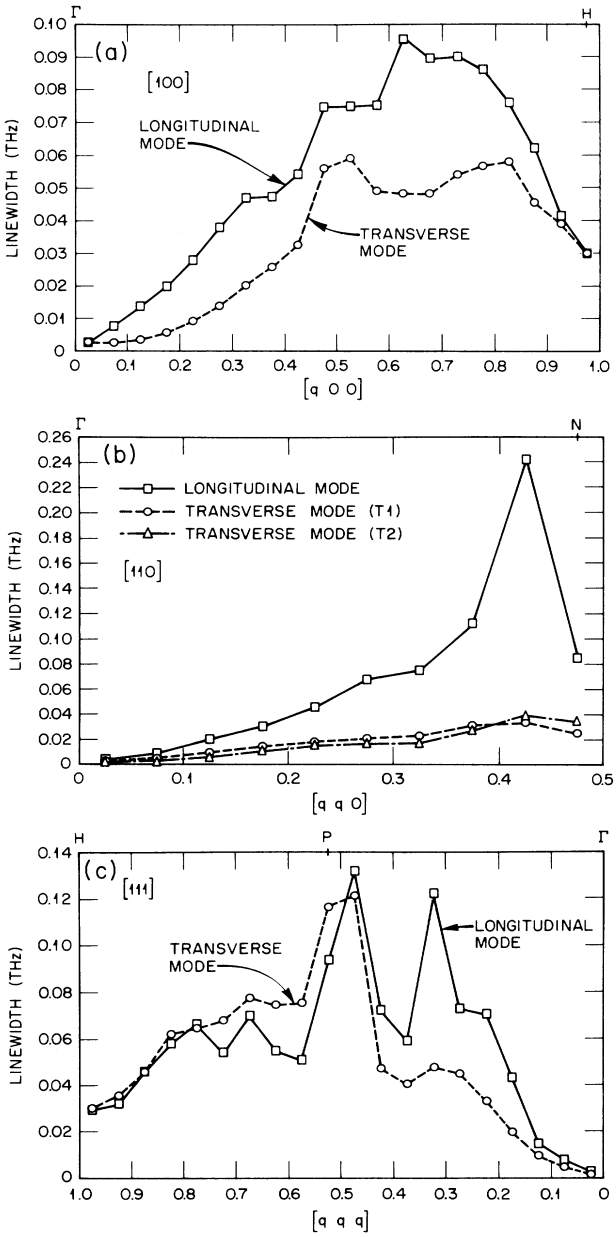

FIG. 2. Calculated phonon linewidth for Ta along symmetry directions. The solid line is for the longitudinal mode while the dashed curves are for the transverse modes. In the [110] direction the two tranverse modes are not degenerate. However, the two sets of linewidths for this direction are essentially equal within the accuracy of the calculation. Note that the ordinate scales are different for the three graphs.

very similar to the case[1,25] of Nb: the only large phonon linewidths are for the longitudinal phonons in the [110] direction [Fig. 2(b)]. The longitudinal-phonon linewidth reaches a peak value of 0.25 THz near the Brillouin-zone boundary at the point N. This maximum in the [110] longitudinal phonons is about half that of the same phonons in Nb. The smaller phonon linewidths for Ta than for Nb is consistent with the values of λ. We do not know of any experiments that have been carried out on the phonon linewidths in Ta. Such measurements in Ta would appear to be very difficult, since the phonon linewidths in Nb were at the limit of the experimental resolution.

The transport spectral function $\alpha^2_{tr}F(\omega)$ is needed to calculate the electrical resistivity in the lowest-order variational approximation. Using Eqs. (5), (6), and (7), we have calculated this spectral function and it is plotted in Fig. 3. This spectral function is smaller than α^2F by almost a factor of 2. In terms of the relative shapes of these two spectral functions, the transverse peak in α^2F is smaller compared to its longitudinal peak than is the case for $\alpha^2_{tr}F$. This is clearly seen from the plot of the ratio $\alpha^2_{tr}F/\alpha^2F$ in Fig. 3 (the dashed curve). This ratio is smaller at the longitudinal peak than at the transverse peak. The ratio also approaches zero as ω goes to zero, in keeping with α^2F going as ω^2 for small ω while $\alpha^2_{tr}F$ goes as ω^4 for small ω.

We have calculated the LOVA electrical resistivity by

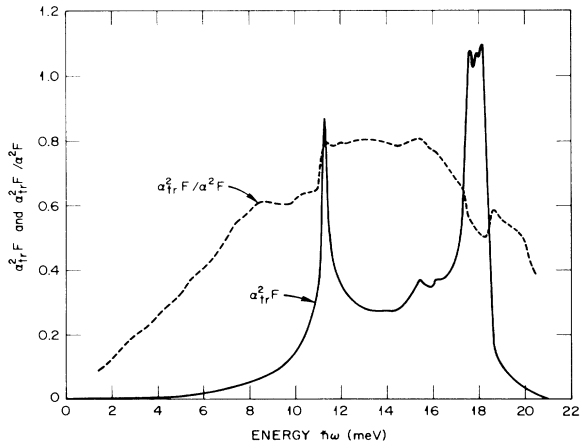

FIG. 3. The transport spectral function $\alpha^2_{tr}F(\omega)$ (solid line) calculated for Ta in the lowest-order variational approximation (LOVA). For comparison with $\alpha^2F(\omega)$, the ratio $\alpha^2_{tr}F(\omega)/\alpha^2F(\omega)$ is plotted as the dashed line.

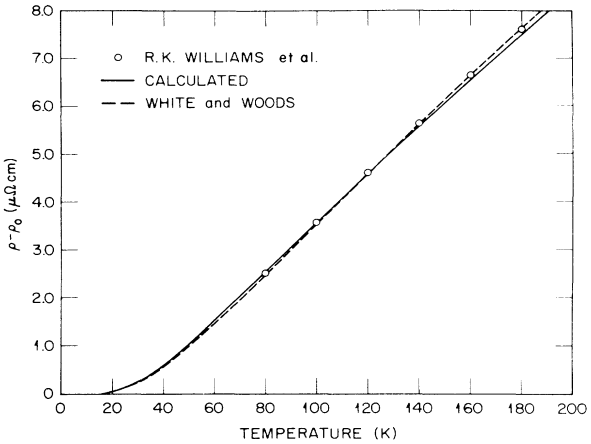

FIG. 4. Temperature dependence of the electrical resistivity of Ta due to the electron-phonon interaction. The solid curve is our calculation with the lowest-order variation approximation (LOVA). The dashed curve gives the experimental results of Ref. 44 while the open circles are experimental results of Ref. 45. In both sets of experimental data we have subtracted the low-temperature impurity resistivity.

means of Eqs. (8) and (9) and have plotted the results in Figs. 4 and 5 as the solid lines. Also displayed are the experimental results[44–46] for the temperature-dependent part of the resistivity, i.e., subtracting off the residual resistivity. The agreement between theory and experiment is remarkable in the temperature range $T_c \leq \Theta_D$, as shown in Fig. 4. We have not carried out calculations with the more refined variational approximations as was done in Refs. 8, 9, and 11. In those papers it was found that the largest corrections in using better distribution functions

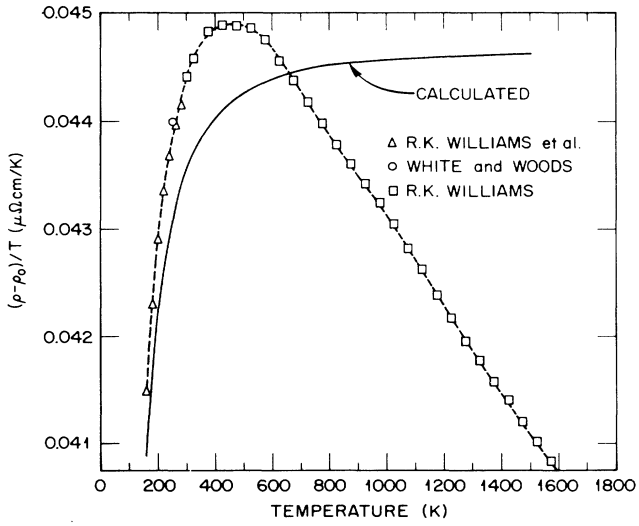

FIG. 5. The temperature-dependent part of the resistivity divided by temperature at high temperature. The solid line is the result of our calculations with LOVA. The experimental results are the circles (Ref. 44), the triangles (Ref. 45), and the squares (Ref. 46). The dashed curve is drawn through the experimental points. Note that the ordinate does *not* begin at zero.

occur at temperatures below Θ_D and the maximum effect is a 20–30 % reduction in $\rho(T)$ at the lowest tempertures. Comparing with the calculations on Nb (Ref. 9) (which is expected to be most nearly like Ta) and taking into account the lower phonon frequencies of Ta, we estimate that a better distribution function would lower the calculated result in Fig. 4 by about 20% at 30 K, about 8% at 60 K, and about 4% at 100 K. Thus, if a better solution to the Boltzmann equation had been obtained, the calculated curve in Fig. 4 would probably lie very slightly below the experimental one below 100 K.

The high-temperature resistivity is shown in Fig. 5. In this temperature range, the LOVA result should be very close to results with better distribution functions. Here we have divided $\rho-\rho_0$ by T. On such a plot, if $\rho-\rho_0$ is proportional to T, as expected at high temperature from theories based on the Boltzmann equation, the curve will approach a horizontal straight line. We see that the LOVA calculation does indeed approach a constant value of 0.0446 $\mu\Omega$ cm/K at temperatures at 1600 K and above. On the other hand, the experimental points reach a maximum at about 450 K. The reason for the decrease of $(\rho-\rho_0)/T$ with T of the experimental data at higher temperatures is not known. A very similar phenomenon is observed in Nb and Pd. We ascribe this high-temperature deviation from linearity to one or more of the following. (1) An increase in the phonon frequencies with increase in temperature. This behavior is atypical, but not impossible. (2) A shift of the Fermi level relative to the structure in the d bands due to the finite width of the Fermi function at high temperature. (3) The smearing of the energy bands due to the finite electron lifetime at high temperature. (4) Changes in the band structure in the vicinity of the Fermi energy due to band shifts resulting from the electron-phonon interaction. Another possibility is that this is the onset of the Mott type of resistivity saturation.[47] All of these effects are interesting but lie outside the scope of this paper.

For temperature up to about 1000 K there is very good agreement of our LOVA calculation and experiment. Note that the ordinate in Fig. 5 does not start at zero. Our calculations are performed within the Bloch-Boltzmann theory, which does not contain the possibility of a high-temperature deviation from linearity. The slope of the resistivity versus temperature curve at high T is proportional to λ_{tr}, which is a measure of the electron-phonon interaction strength.[9] The good agreement between theory and experiment up to where resistivity deviation from linearity begins to have an effect indicates that our calculated λ of 0.88 is probably correct. This is in contrast with λ of 0.70 determined from tunneling, which is compromised by the fact that the unknown Coulomb coupling μ^* enters into the analysis.

We can compare the tunneling λ with the high-temperature resistivity in the following manner. We have taken $\alpha^2F(\omega)$ from tunneling[32,33] and, at each ω, multiplied it by the ratio $\alpha^2_{tr}F(\omega)/\alpha^2F(\omega)$ from our calculations. Assuming that our calculated ratio is correct even if the individual magnitudes might not be, we thus obtain an $\alpha^2_{tr}F(\omega)$ based on tunneling. This modified spectral function was used to calculate the maximum value of

ρ/T. We find a value of 0.034 $\mu\Omega$ cm/K which is 23% low (it is below the lowest ordinate value in Fig. 5) compared to experiment. This indicates that (if our calculated ratio of α_{tr}^2/α^2 is correct) the tunneling λ and the high-temperature resistivity are not consistent with each other.

On the other hand, the λ from electronic specific-heat measurements of 0.95 to 1.14 is consistent with the measured high-temperature resistivity λ and our calculated λ of 0.88. We again want to emphasize that the analysis leading to a measured superconducting λ involves the *ad hoc* μ^*. The specific-heat λ and the electrical-resistivity λ do not involve μ^*.

Because of the disagreement on the longitudinal peak between the calculated α^2F and the α^2F from tunneling, it would be interesting to compare the calculations of a different spectral function with what is obtained from experiment. Since the electrical resistivity depends on α_{tr}^2F only in a gross way, the detailed structure of α_{tr}^2F cannot be obtained from resistivity measurements. However, point-contact spectroscopy gives detailed information on the point-contact spectral function $G(\omega)$. We have carried out the calculation of this function for Ta using Eqs. (10)–(12) and plotted the result in Fig. 6 as the solid line. A comparison of the magnitude of $G(\omega)$ with $\alpha^2F(\omega)$ is not very meaningful [$G(\omega)$ is smaller because the geometrical structure factor cuts out all small-angle scattering]. However, a comparison of the shapes of the two functions can be achieved by plotting the ratio $G(\omega)/\alpha^2F(\omega)$, the dashed line in Fig. 6. This line is not constant, indicating that the two functions do not have the same shape [in fact the variation of the ratio $G(\omega)/\alpha^2F(\omega)$ in Fig. 6 is about the same as the variation of $\alpha_{tr}^2F(\omega)/\alpha^2F(\omega)$ in Fig. 3]. However, G/α^2F has about the same value at the transverse peak as at the longitudinal peak (unlike the situation with α_{tr}^2F/α^2F) indicating that, first, the two peaks occur at the same frequencies for these functions [as also for $\alpha_{tr}^2F(\omega)$], and second, the ratio of the heights of the two peaks is about the same for $G(\omega)$ as for $\alpha^2F(\omega)$. That is, $G(\omega)$ has a large longitudinal peak compared to the transverse peak just as in the case of $\alpha^2F(\omega)$. We are not aware of any

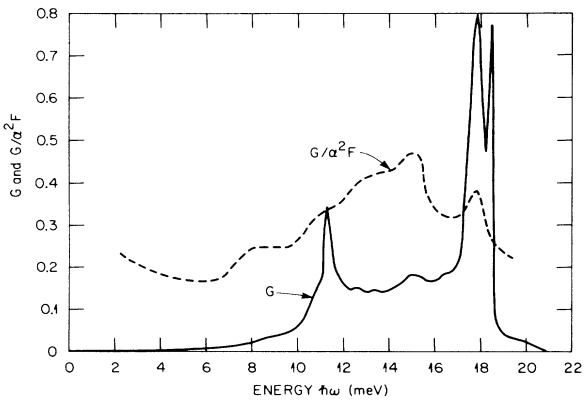

FIG. 6. The Kulik point contact spectral function $G(\omega)$ calculated for Ta (solid curve). For comparison with $\alpha^2F(\omega)$, the ratio $G(\omega)/\alpha^2F(\omega)$ is plotted as the dashed line.

point-contact measurements that have been made on Ta. It is important to have such results to see if, in the experimental $G(\omega)$, the longitudinal peak is suppressed compared to the calculations, as in the case of α^2F.

IV. CONCLUSIONS

The most important results are (1) that the calculated quantities for Ta are remarkably similar to those of Nb where comparison can be made, and (2) that (as in the case of Nb) the calculated results with the rigid-muffin-tin approximation for the electron-phonon interaction effects in the electronic specific heat and the high-temperature resistivity agree well with experiment. For the superconducting properties (α^2F from superconducting tunneling and λ from T_c) there is not as good agreement between the calculated and measured quantities. However, for the analysis of the superconducting properties it is necessary to use an *ad hoc* constant value μ^* for the Coulomb repulsion.

Our calculated $\alpha^2F(\omega)$ agrees well with that obtained from superconducting tunneling with regard to the location of the two peaks and the size and shape of the transverse peak. However, as in the case of Nb, our calculated longitudinal peak for Ta is much larger in magnitude than that obtained from tunneling. Our calculated λ is approximately 25% larger than the λ from superconducting tunneling, which is consistent with the discrepancy in α^2F. On the other hand, our calculated high-temperature resistivity is in good agreement with experiment, indicating that our calculated λ_{tr} is correct. In fact, we show that the experimental tunneling $\alpha^2F(\omega)$, adjusted to take into consideration the difference in shape between $\alpha^2F(\omega)$ and $\alpha_{tr}^2F(\omega)$, gives a high-temperature resistivity that is about 23% too low.

Similar to the case of Nb, a peak of relatively large size occurs in the linewidth for longitudinal phonons in the [110] direction near the zone boundary. Unfortunately, there are no experimental determinations of the phonon linewidth in Ta, nor does it seem to be feasible. However, our good agreement with high-temperature resistivity and low-temperature electronic specific heat in Ta together with the good agreement with experiment of both the calculated phonon linewidth[1,25] and the calculated high-temperature resistivity[9] of Nb, seem to indicate that these calculations with rigid-muffin-tin potentials describe the electron-phonon interaction properly, at least for these quantities. This suggests that the calculated $\alpha^2F(\omega)$ for the transition metals may be closer to the true α^2F than is that deduced from superconducting tunneling. It may be, as was suggested in Ref. 25, that, because of a combination of low group velocity and short lifetime of the electron quasiparticles that make the major contribution to the longitudinal peak in α^2F, the tunneling experiments do not measure the full contribution to the longitudinal peak. Our overestimate of T_c remains a puzzle, but our determination of T_c requires an *ad hoc* μ^*. The treatment of the Coulomb interaction (μ^*) in determining T_c certainly is not at the same level of sophistication as is the model in determining λ.

The conclusion that the calculated electron-phonon in-

teraction effects using the rigid-muffin-tin potential are in good agreement with experiment is similar to the conclusions reached in Refs. 48 and 49. These conclusions are in disagreement with those of Ref. 15.

The calculated point-contact spectral function $G(\omega)$ is similar in shape to the calculated α^2F with the same large ratio of longitudinal to transverse peak heights. This is quite different from the case in the alkali metals[13] where the ratio of longitudinal to transverse peak height is quite different for $G(\omega)$ from $\alpha^2F(\omega)$. For both Na and K, there is good agreement between theory[13,14] and experiment.[50] It is important to have experimental results on point-contact spectra of Ta to compare with our calculations.

ACKNOWLEDGMENTS

Mr. Al-Lehaibi received support from the Saudi Arabian Government and was working on his Ph.D. thesis based on much of this work at the time of his death. We are indebted to Dr. T. J. Watson Yang for providing the relativistic modification in the KKR program used in this work and for adapting some of the Oak Ridge programs to run on the computer system at Indiana University. We wish to than Dr. L. L. Boyer, Dr. B. M. Klein, and Dr. D. A. Papaconstantopoulos for providing the self-consistent potential for Ta and Dr. R. K. Williams for providing his unpublished high-temperature resistivity data on Ta. Work at Indiana University was supported in part by National Science Foundation Grant No. DMR 81-17013. Work at Oak Ridge was supported by the Division of Materials Sciences, U.S. Department of Energy, under Contract No. DE-AC05-840R21400 with the Martin Marietta Energy Systems, Inc. One of us (JCS) wishes to thank the Metals and Ceramics Division of Oak Ridge National Laboratory for its hospitality while part of this work was carried out.

---

*Deceased.

[1]W. H. Butler, F. J. Pinski, and P. B. Allen, Phys. Rev. B **19**, 3708 (1979).

[2]A. B. Meador and W. E. Lawrence, Phys. Rev. B **15**, 1850 (1977).

[3]F. S. Khan, P. B. Allen, W. H. Butler, and F. J. Pinski, Phys. Rev. B **26**, 1538 (1982).

[4]B. Bhattacharyya and J. C. Swihart, Phys. Rev. B **30**, 1656 (1984).

[5]P. G. Tomlinson and J. C. Swihart, Phys. Rev. B **19**, 1867 (1979).

[6]B. K. Bhattacharyya and J. C. Swihart, J. Phys. F **14**, 1651 (1984).

[7]H. K. Leung, F. W. Kus, N. McKay, and J. P. Carbotte, Phys. Rev. B **16**, 4358 (1977).

[8]P. G. Tomlinson, Phys. Rev. B **19**, 1893 (1979).

[9]F. J. Pinski, P. B. Allen, and W. H. Butler, Phys. Rev. B **23**, 5080 (1981).

[10]T. P. Beaulac, P. B. Allen, and F. J. Pinski, Phys. Rev. B **26**, 1549 (1982).

[11]M. P. Pepchinski and J. C. Swihart (unpublished).

[12]I. O. Kulik, A. N. Omel'yanchuk, and R. I. Shekhter, Fiz. Nizk. Temp. **3**, 1543 (1977) [Sov. J. Low Temp. Phys. **3**, 740 (1977)].

[13]M. Ashraf and J. C. Swihart, Phys. Rev. B **25**, 2094 (1982).

[14]A. H. MacDonald and C. R. Leavens, Phys. Rev. B **26**, 4293 (1982). In this paper the authors completely misstate the conclusions stated in Ref. 13.

[15]D. Glötzel, D. Rainer, and H. R. Schober, Z. Phys. B **35**, 317 (1979).

[16]W. L. McMillan and J. M. Rowell, in *Superconductivity,* edited by R. D. Parks (Marcel Dekker, New York, 1969), Vol. I, p. 561.

[17]P. G. Tomlinson and J. P. Carbotte, Phys. Rev. B **13**, 4738 (1976).

[18]J. C. Swihart and D. G. Garrett (unpublished).

[19]H. K. Leung, J. P. Carbotte, D. W. Taylor, and C. R. Leavens, Can. J. Phys. **54**, 1585 (1976).

[20]J. Zasadzinski, D. M. Burnell, E. L. Wolf, and G. B. Arnold, Phys. Rev. B **25**, 1622 (1982).

[21]B. N. Harmon and S. K. Sinha, Phys. Rev. B **16**, 3919 (1977).

[22]M. Peter, J. Ashkenazi, and M. Dacorogna, Helv. Phys. Acta **50**, 267 (1977).

[23]G. B. Arnold, J. Zasadzinski, J. W. Osmun, and E. L. Wolf, J. Low Temp. Phys. **40**, 225 (1980).

[24]B. Robinson, T. H. Geballe, and J. M. Rowell, in *Superconductivity in d- and f-Band Metals,* edited by D. H. Douglas (Plenum, New York, 1976), p. 381.

[25]W. H. Butler, H. G. Smith, and N. Wakabayashi, Phys. Rev. Lett. **39**, 1004 (1979); N. Wakabayashi, Phys. Rev. B **33**, 6771 (1986).

[26]L. Y. L. Shen, in *Superconductivity in d- and f-Band Metals,* Proceedings of the Conference on Superconductivity in *d*- and *f*-Band Metals, AIP Conf. Proc. No. 4, edited by D. H. Douglas (AIP, New York, 1972), p. 31.

[27]J. Bardeen, Phys. Rev. **52**, 688 (1937).

[28]W. H. Butler, in *Electronic Structure and Properties,* edited by F. Y. Fradin (Academic, New York, 1981), p. 165–222.

[29]W. H. Butler, Can. J. Phys. **60**, 735 (1982).

[30]H. Winter, J. Phys. F **11**, 2283 (1981).

[31]W. H. Butler, in *Physics of Transition Metals—1980,* Inst. Phys. Conf. Ser. No. 55, edited by P. Rhodes (IOP, Bristol, England, 1981), pp. 505–518.

[32]L. Y. L. Shen, Phys. Rev. Lett. **24**, 1104 (1970).

[33]E. L. Wolf, R. J. Noer, D. Burnell, Z. G. Khim, and G. B. Arnold, J. Phys. F **11**, L23 (1981).

[34]W. H. Butler, J. J. Olsen, J. S. Faulkner, and B. L. Gyorffy, Phys. Rev. B **14**, 3823 (1976).

[35]L. L. Boyer, D. A. Papaconstantopoulos, and B. M. Klein, Phys. Rev. B **15**, 3685 (1977).

[36]D. D. Koelling and B. N. Harmon, J. Phys. C **10**, 3107 (1977).

[37]L. L. Boyer and B. M. Klein, Int. J. Quantum. Chem. **59**, 511 (1975).

[38]A. D. B. Woods, Phys. Rev. **136**, 781 (1964).

[39]R. D. Worley, M. W. Zemansky, and H. A. Boorse, Phys. Rev. **99**, 447 (1955).

[40]Y. L. Shen, USAEC Report No. UCRL 16117, 1965 (unpublished).

[41]P. B. Allen and R. C. Dynes, Phys. Rev. B **12**, 905 (1975).

[42]L. L. Boyer, B. M. Klein, and D. A. Papaconstantopoulos,

Ferroelectrics **16**, 291 (1977).
[43]R. W. Reed and A. C. Boyer, J. Low Temp. Phys. **24**, 35 (1976).
[44]G. K. White and S. B. Woods, Philos. Trans. R. Soc. London, Ser. A **251**, 273 (1959).
[45]R. K. Williams, R. S. Graves, T. L. Hebble, D. L. McElroy, and J. P. Moore, Phys. Rev. B **26**, 2932 (1982).
[46]R. K. Williams (private communication).
[47]J. C. Swihart and W. H. Butler, in *Condensed Matter Theories,* edited by P. Vashishta *et al.* (Plenum, New York, in press), Vol. 2.
[48]P. B. Allen, T. P. Beaulac, F. S. Kahn, W. H. Butler, F. J. Pinski, and J. C. Swihart, in *Materials Research Society Proceedings: Computer Based Microscopic Description of the Structure and Properties of Materials,* edited by J. Q. Broughton, W. Krakow, and S. T. Pantelides (MRS, Boston, 1986).
[49]P. B. Allen, T. P. Beaulac, F. S. Kahn, W. H. Butler, F. J. Pinski, and J. C. Swihart, Phys. Rev. B **34**, 4331 (1986).
[50]A. G. M. Jansen, J. H. van den Bosch, H. van Kempen, J. H. J. M. Ribot, P. H. H. Smeets, and P. Wyder, J. Phys. F **10**, 265 (1980).